Mode interactions in the one-sided and the symmetric model of directional solidification

Peter Haug
Institute for Information Sciences, University of Tübingen, Köstlinstrasse 6, D-7400 Tübingen, Federal Republic of Germany
(Received 11 April 1989)

We analyze the interactions of the first and second mode arising in the one-sided and the symmetric model of directional solidification of a dilute binary alloy if a planar interface loses stability and stationary cellular structures are formed. Algebraic bifurcation equations for the coupled amplitudes of the two unstable modes are derived from the nonlinear equations of motion with the interface velocity as a control parameter. The transitions from planar to cellular interfaces are described in terms of normal forms and bifurcation diagrams. Thereby we predict that each of the two bifurcating solution branches can show hysteretic behavior and that for suitable values of the parameters involved there exist tertiary Hopf bifurcations to time-periodic interface shapes. The results are compared to recent numerical work and the nature of the one-sided limit is discussed.

I. INTRODUCTION

In recent years directional solidification[1-13] has become a paradigm for the formation and evolution of spatiotemporal structures in nonlinear systems.[14] In general, these structures appear if an externally controllable parameter passes through a critical value so that a balance existing between competing forces breaks down. The system then restabilizes in a more complex space- and time-dependent configuration. Mathematically, such a *bifurcation*[15] occurs if the real part of an eigenvalue of the linearized system passes through zero from negative values. A zero eigenvalue leads to stationary solutions whereas a pair of imaginary eigenvalues gives rise to time-periodic structures. Variation of an extra parameter may change the eigenvalue structure and thus can lead to multiple bifurcations which induce interactions of different modes. If the spectrum of the linearized system is discrete, then only a finite number of modes can interact in the vicinity of a multiple bifurcation point. This is always the case in systems with finite spatial extension. Typically, the extra parameter that induces mode interactions is given by some characteristic length as, e.g., the aspect ratio in convection systems.

In the field of directional solidification the role of this extra parameter is played by the width of the sample.[6,10-12] If this width is finite, then the appropriate boundary conditions are those of no solute flux across the side walls. Then, as we shall see, the wavelength and the bifurcation behavior of the evolving stationary cellular interfaces depend on the width of the sample. If the sample is taken to have an infinite width, then there should be an other selection mechanism for the wavelength of the interface structure. However, in numerical simulations of the solidification system the computational domain always has to be finite. Hence they all deal, in fact, with a finite sample width and, therefore, yield interactions of a finite number of modes. In recent years several papers on such numerical work about mode interactions have been published.[6-9] A systematic analytical approach to solve a simplified one-sided model with finite sample width has been made in Ref. 10 by use of *imperfect bifurcation theory*.[15,16] In the present paper we want to extend this analysis to a more realistic model for the one-sided and the symmetric case. Thereby we restrict ourselves to interactions of the first and the second mode. We begin, in Sec. II, with the equations describing the two-dimensional system of directional solidification with nonflux boundary conditions at the side walls and the interface velocity as control parameter. In Sec. III we derive a system of evolution equations for the Fourier amplitudes of the interface which is reduced further to algebraic bifurcation equations describing the branching of stationary cellular interfaces. In Sec. IV a linear stability analysis is performed. In Sec. V we determine all degenerate interactions of the first and the second mode for both the one-sided and the symmetric model, and express the results in terms of normal forms and bifurcation diagrams. In the discussion in Sec. VI we compare our analysis with other results, comment on the nature of the one-sided limit, and make some suggestions for future work.

II. DIRECTIONAL SOLIDIFICATION

Consider a thin, two-dimensional sample of a dilute binary alloy which is pulled, at a velocity V, through a fixed constant temperature gradient towards the region of lower temperature (Fig. 1). Hence the interface separating the solid and liquid phases moves through the material during the process of solidification. At low pulling velocities this interface is flat, but as V increases beyond some critical value the planar interface becomes unstable and evolves into cellular morphologies of definite wavelength and amplitude. This instability is the result of the competition between the destabilizing effect of the solute diffusion and the stabilizing forces of surface tension and the temperature gradient.[1]

It is often assumed that the temperature distribution is given by the imposed gradient alone,[7-13] which implies

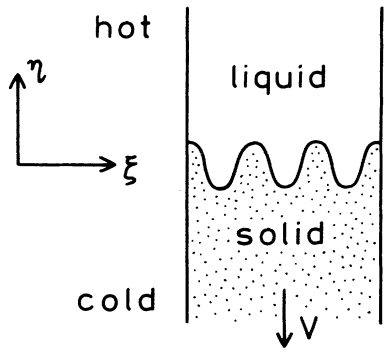

FIG. 1. Schematic representation of the two-dimensional system of directional solidification.

that the latent heat released at the interface is negligible and the thermal conductivities of the two phases are equal. Then the solidification process is primarily governed by solute diffusion, and so one often speaks of a *solutal model*. In the frame of reference moving with the interface at velocity V, the diffusion of the solute concentration $\tilde{c}^{L,S}(\tilde{\xi},\tilde{\eta},t)$ in the liquid (L) and solid (S) part, respectively, is described by the equations

$$\mathcal{D}\Delta\tilde{c}^{L}+V\tilde{c}^{L}_{\tilde{\eta}}-\tilde{c}^{L}_{t}=0 \quad \text{for } \tilde{\eta}>\tilde{s}(\tilde{\xi},t) , \tag{1}$$

$$\mathcal{D}_S\Delta\tilde{c}^{S}+V\tilde{c}^{S}_{\tilde{\eta}}-\tilde{c}^{S}_{t}=0 \quad \text{for } \tilde{\eta}<\tilde{s}(\tilde{\xi},t) , \tag{2}$$

where $\tilde{\eta}$ is the coordinate in the direction of increasing temperature, $\tilde{\xi}$ is the coordinate perpendicular to $\tilde{\eta}$, $\mathcal{D}$ and $\mathcal{D}_S$ are the diffusion coefficients in the melt and solid, respectively, and $\tilde{s}(\tilde{\xi},t)$ describes the position of the interface. The two-dimensional Laplace operator is denoted by Δ, t is time, and $\tilde{c}_{\tilde{\eta}}$ and $\tilde{c}_t$ denote partial derivatives. At the interface $\tilde{\eta}=\tilde{s}(\tilde{\xi},t)$ the Gibbs-Thomson relation has to be satisfied, which reduces here to

$$\tilde{c}^{L}=\frac{c_\infty}{\kappa}-\frac{G}{-\tilde{m}}\tilde{s}-\frac{T_m\Gamma}{-\tilde{m}}\mathcal{H}(\tilde{s}) , \tag{3}$$

where c_∞ is the solute concentration far away from the interface, κ is the segregation coefficient ($0<\kappa<1$), G is the temperature gradient, $\tilde{m}<0$ is the slope of the liquidus line in the phase diagram, T_m is the melting temperature of the pure material (i.e., for $\tilde{c}=0$), Γ is the capillary length, and finally

$$\mathcal{H}(\tilde{s})=-\tilde{s}_{\tilde{\xi}\tilde{\xi}}/(1+\tilde{s}^{\,2}_{\tilde{\xi}})^{3/2}$$

is the curvature of the interface at $\tilde{\eta}=\tilde{s}(\tilde{\xi},t)$. Conservation of matter across the interface implies

$$-(V+\tilde{s}_t)J(\tilde{c}^{L})+\mathcal{D}(\tilde{s}_{\tilde{\xi}}\tilde{c}^{L}_{\tilde{\xi}}-\tilde{c}^{L}_{\tilde{\eta}})-\mathcal{D}_S(\tilde{s}_{\tilde{\xi}}\tilde{c}^{S}_{\tilde{\xi}}-\tilde{c}^{S}_{\tilde{\eta}})=0 \quad \text{for } \tilde{\eta}=\tilde{s}(\tilde{\xi},t) , \tag{4}$$

where $\tilde{c}^{L}$ and $\tilde{c}^{S}$ denote the concentrations on the liquid and solid sides of the interface, respectively, and $J(\tilde{c}^{L})\equiv\tilde{c}^{L}-\tilde{c}^{S}$ is the concentration jump at the interface.

At the side walls of the sample we impose nonflux boundary conditions for the concentration field

$$\tilde{c}_{\tilde{\xi}}=0 \quad \text{for } \tilde{\xi}=0,L , \tag{5}$$

where L is the width of the sample, and for $\tilde{\eta}\to\pm\infty$ we have

$$\lim_{\tilde{\eta}\to\pm\infty}\tilde{c}=c_\infty . \tag{6}$$

To simplify the model, some further approximations are widely used in the literature.

First, the concentration jump J is expanded into a Taylor series around the concentration $\tilde{c}_0$ at the liquid side of a flat interface,

$$J(\tilde{c}^{L})=J(\tilde{c}_0)+J'(\tilde{c}_0)(\tilde{c}^{L}-\tilde{c}_0)+\cdots .$$

Taking into account only the constant term, we get $J(\tilde{c}^{L})=(1-\kappa)c_\infty/\kappa$.[5,10–13] If we add the linear term and additionally take the phase diagram of the alloy to be linear, then the above Taylor series becomes a linear function given by $J(\tilde{c}^{L})=(1-\kappa)\tilde{c}^{L}$.[6–9]

The second type of approximation concerns the diffusivities in the two phases. Neglecting solute diffusion in the solid phase, i.e., assuming $\mathcal{D}_S=0$, leads to the so-called *one-sided model*, whereas assuming $\mathcal{D}=\mathcal{D}_S$ results in a *symmetric model*.

The bifurcations of the planar interface to stationary cellular morphologies in the model with $J=(1-\kappa)c_\infty/\kappa$ and $\mathcal{D}_S=0$ have been analyzed in Ref. 10, but in numerical approaches usually $J=(1-\kappa)\tilde{c}^{L}$ is used.[6–9] Taking $J=$const means in terms of the phase diagram[1,11] that the solidus and the liquidus lines are parallel locally around the temperature of the planar interface. But in a linear phase diagram the solidus and the liquidus lines can be parallel only if they coincide, but then the segregation coefficient κ equals 1. So in this sense, not strictly, the approximation $J=$const corresponds to a limit $\kappa\to1$.

In the following we want to analyze the qualitative, local bifurcation behavior of the models with $J=(1-\kappa)\tilde{c}^{L}$ in the case where the first and second mode interact nonlinearly.

To minimize the number of parameters involved we begin the analysis with a rescaling of the variables. With $c^{L,S}=\tilde{c}^{L,S}/c_\infty$, $\eta=\alpha\tilde{\eta}$, $\xi=\alpha\tilde{\xi}$, and $\tau=\alpha^2\mathcal{D}t$ the system (1)–(6) transforms into

$$\Delta c^{L}+\nu c^{L}_{\eta}-c^{L}_{\tau}=0 \quad \text{for } \eta>s(\xi,\tau) , \tag{7}$$

$$R\,\Delta c^{S}+\nu c^{S}_{\eta}-c^{S}_{\tau}=0 \quad \text{for } \eta<s(\xi,\tau) , \tag{8}$$

$$c^{L}=\frac{1}{\kappa}-s-\frac{1}{u}\mathcal{H}(s) \quad \text{for } \eta=s(\xi,\tau) , \tag{9}$$

$$-(\nu+s_\tau)(1-\kappa)c^{L}+s_\xi c^{L}_{\xi}-c^{L}_{\eta}-R\,(s_\xi c^{S}_{\xi}-c^{S}_{\eta})=0 \quad \text{for } \eta=s(\xi,\tau) , \tag{10}$$

$$c_\xi=0 \quad \text{for } \xi=0,\ \xi=b , \tag{11}$$

$$\lim_{\eta\to\pm\infty}c=1 , \tag{12}$$

$$c^{S}=\kappa c^{L} \quad \text{for } \eta=s(\xi,\tau) . \tag{13}$$

Here, the various new parameters are defined as follows:

$$\alpha=\frac{G}{-\tilde{m}c_\infty}>0,\quad \nu=\frac{V}{\alpha\mathcal{D}}>0\ ,$$

$$R=\frac{\mathcal{D}_S}{\mathcal{D}},\quad u=\frac{\tilde{m}^2c_\infty^2}{GT_m\Gamma}>0,\quad b=\alpha L\ .$$

In virtue of the boundary conditions (9) and (10) the system (7)–(13) is highly nonlinear. It always possesses a trivial solution with a planar interface $s(\xi,\tau)=0$ which is given by

$$c_0^L=1+\frac{1-\kappa}{\kappa}\exp(-\nu\eta)\quad\text{for } \eta>0\ ,$$

$$c_0^S=1\quad\text{for } \eta<0\ .$$

III. DERIVATION OF BIFURCATION EQUATIONS

Following Ref. 10 we begin the analysis of (7)–(13) with the derivation of a system of evolution equations for the Fourier modes of the interfacial displacement $s(\xi,\tau)$. Because of the nonflux boundary conditions (11) the interface can be expanded in a cosine series[10,11]

$$s(\xi,\tau)=\sum_{m=0}^{\infty}\epsilon_m(\tau)\cos(m\sqrt{u}\,k_0\xi)\ ,$$

where ϵ_m is real and

$$k_0=\pi/(b\sqrt{u}\,)=(\pi/L)(T_m\Gamma/G)^{1/2}>0$$

is the fundamental wave number depending on the width L of the sample. Using a quasistationary approximation[1] the solute concentrations c^L and c^S can be expanded into a formal Taylor series with respect to $\epsilon=(\epsilon_0,\epsilon_1,\epsilon_2,\ldots)$ around the planar interface solution $\epsilon_m\equiv0$, where the Taylor coefficients are uniquely determined by Eqs. (7), (8), (9), (12), and (13). Substituting this Taylor series into Eq. (10) we obtain an infinite system of coupled nonlinear first-order differential equations for the ϵ_m,[5,11]

$$\dot{\epsilon}_m=\sum_{j=1}^{\infty}\sum_{\substack{r_1,\ldots,r_j\in Z\\ r_1\le\cdots\le r_j\\ \sum_n r_n=m}}a^{(m)}_{r_1,\ldots,r_j}\epsilon_{|r_1|}\cdots\epsilon_{|r_j|}\ , \tag{14}$$

i.e.,

$$\dot{\epsilon}_m=a_m\epsilon_m+M_m(\epsilon),\quad i=0,1,2,\ldots$$

where the $a_m\equiv a^{(m)}_m$ are the (real) eigenvalues of the linearized system and the M_m describe the nonlinear effects.

The coefficients $a^{(m)}_{r_1,\ldots,r_j}$ depend on ν and the system parameters u, κ, R, and k_0 and can be calculated explicitly to any desired order using computer algebra systems such as SMP.[11] A formula for these coefficients is given in the Appendix. The trivial solution $\epsilon_m=0$ of (14) represents the planar interface and is stable if $a_i<0$ for all i, which is the case for sufficiently small ν (cf. Sec. IV). As ν increases and passes through a critical value ν_c, some of the eigenvalues a_m of the linearization of the system (14) go through zero from negative values. Then, the planar interface loses stability and the system encounters bifurcation to cellular steady-state interfaces in virtue of the nonlinear terms M_m in (14). Because there are no primary Hopf bifurcations, we confine ourselves to stationary solutions with $\dot{\epsilon}_m=0$ in (14). As shown in Ref. 10 we use a Lyapunov-Schmidt reduction to reduce the problem of finding solutions of (14) near the onset of instability of the planar interface to the problem of solving a single equation: Suppose that $a_n=0$ is the first eigenvalue going through zero for $\nu=\nu_c$, so that $a_m<0$ for $m\neq n$. Then the nth equation in (14) is degenerate because its linear part vanishes. According to the implicit function theorem, the nondegenerate equations in (14), those with $m\neq n$, can be solved with respect to the ϵ_m, $m\neq n$, thus leading to $\epsilon_m=\epsilon_m(\epsilon_n)$. Substituting these expressions into the remaining degenerate equation with $m=n$ yields a single algebraic bifurcation equation for the stationary amplitude ϵ_n,

$$B(\epsilon_n,\nu)\equiv M_n(\epsilon(\epsilon_n))=0\ , \tag{15}$$

with $B(0,\nu)=0$ and $\partial B(0,\nu_c)/\partial\epsilon_n=0$. In virtue of the symmetry of Eqs. (7)–(13) with respect to reflections at the axis $\xi=b/2$ and the nonflux boundary conditions (11), Eq. (15) takes, following Ref. 17, the form

$$B(x,\nu)=xh(x^2,\nu)=0\ ,$$

where $x\equiv\epsilon_n$ is the amplitude of the mode becoming unstable first and $h(x^2,\nu)$ is some smooth function satisfying $h(0,\nu_c)=0$. The Taylor coefficients of B at $x=0$ and $\nu=\nu_c$ can be calculated explicitly in terms of the coefficients $a^{(m)}_{r_1,\ldots,r_j}$.[10]

In Sec. IV we will see that it is possible that two modes ϵ_n and ϵ_{n+1} become unstable simultaneously at $\nu=\nu_c$. Then we obtain two coupled equations for the amplitudes ϵ_n and ϵ_{n+1} of the form[17]

$$\begin{aligned}B^{(1)}(x,y,\nu)&=xa(x^2,y^2,\nu)+x^ny^nb(x^2,y^2,\nu)=0\ ,\\ B^{(2)}(x,y,\nu)&=yc(x^2,y^2,\nu)+x^{n+1}y^{n-1}d(x^2,y^2,\nu)=0\ ,\end{aligned} \tag{16}$$

where $x\equiv\epsilon_n$, $y\equiv\epsilon_{n+1}$, $n\ge1$, and a, b, c, and d are smooth functions. The form of (16) and, therefore, the resulting bifurcation behavior depends on the wave numbers n and $n+1$ of the two unstable modes. Of course, B, $B^{(1)}$, and $B^{(2)}$ also depend on the system parameters u, κ, R, and k_0,

IV. LINEAR STABILITY ANALYSIS

As we have seen in Sec. III, the planar interface loses stability as ν increases if one or more of the eigenvalues a_m go through zero from negative values. The eigenvalues are given by

$$a_n=F_1(n)q(n)-F_1(n)\nu(1-\kappa)+RG_1(n)p(n)-\nu^2(1-\kappa)$$

with

$$F_1(n)=\nu\frac{1-\kappa}{\kappa}-1-n^2k_0^2\ ,$$

$$G_1(n)=-\kappa(1+n^2k_0^2)\,,$$
$$q(n)=\frac{\nu}{2}+\left[\frac{\nu^2}{4}+un^2k_0^2\right]^{1/2}\,, \tag{17}$$
$$p(n)=-\frac{\nu}{2R}+\left[\frac{\nu^2}{4R^2}+un^2k_0^2\right]^{1/2}$$

from which we obtain the neutral stability curve $C(u,\kappa,R)$ depicted in Fig. 2. This curve is closed and convex and expands when u is increased. For decreasing u the curve shrinks and vanishes for u being sufficiently small. When κ increases, then $C(u,\kappa,R)$ shrinks and for increasing R the curve shrinks, too. Qualitatively the neutral stability curve is the same as for the simpler model analyzed in Ref. 10.

To predict the bifurcation behavior of the system near the onset of instability we have to know which mode becomes unstable first as ν increases. For fixed κ and R we get in the same way as in Ref. 10 a subdivision of the (k_0,u) plane into disjoint regions R_n, such that for (k_0,u) lying in R_n the nth mode is the first one becoming unstable when ν is increased, see Fig. 3. If (k_0,u) lies on a boundary curve D_n, above the point P_n, the modes n and $n+1$ become unstable simultaneously as the first ones. Outside the regions R_n there is no instability of the planar interface. Qualitatively this subdivision is the same as for the model of Ref. 10, being a consequence of the geometry of the neutral stability curve $C(u,\kappa,R)$. But, naturally, the positions of these regions R_n change with the values of κ and R, so $R_n=R_n(\kappa,R)$.

V. (1,2) INTERACTIONS

In the literature work on the system (7)–(13) usually is restricted to the special cases $R=0$ and $R=1$, i.e., to the one-sided and the symmetric models, respectively. Also, mostly, work is concentrated on the situation, where the mode number 1, corresponding to $\cos(\sqrt{u}\,k_0\xi)$, is the first one becoming unstable. In virtue of the geometry of the neutral stability curve the mode number 2, corresponding to $\cos(2\sqrt{u}\,k_0\xi)$, becomes unstable next when ν is increased further. In such a situation these two modes interact nonlinearly, which is called *(1,2) interactions.*

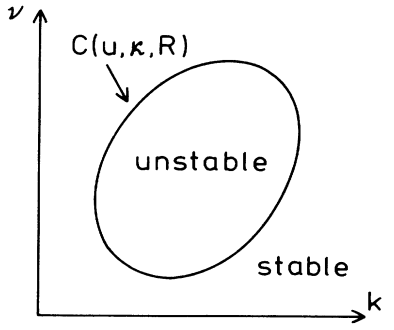

FIG. 2. Neutral stability curve $C(u,\kappa,R)$ showing the critical interface velocity ν depending on the wave number k.

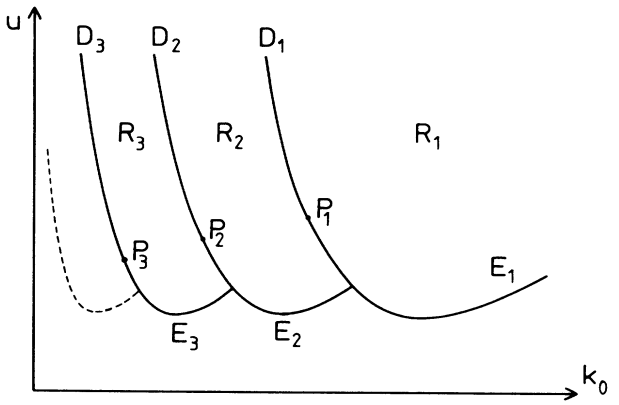

FIG. 3. Division of the (k_0,u) plane indicating the critical modes. For (k_0,u) lying in region R_n, the mode number n becomes unstable first for increasing interface velocity ν and thus determines the wavelength of the bifurcating cellular interface. Naturally, the exact position of these regions depends on the values of κ and R.

However, one should be aware that, because of the special structure of (16), the (1,2) interactions are very different from all other $(n,n+1)$ interactions with $n\geq 2$. For $n\geq 2$ we obtain from (16) two *pure-mode* solution branches with $x=0$, $c(0,y^2,\nu)=0$ and $y=0$, $a(x^2,0,\nu)=0$. They bifurcate from the trivial solution $x=y=0$ and never intersect. In the case $n=1$ there is no pure-mode solution with $y=0$, and the solution branch corresponding to the bifurcation of the first mode off the trivial solution possibly connects in a secondary bifurcation with the $x=0$ pure-mode solution.

In the following, we want to analyze local (1,2) interactions for the system (7)–(13) with $R=0$ and 1 by applying *imperfect bifurcation theory*[15,16] as outlined in Ref. 10. Thereby, we concentrate on the search for *degeneracies*, i.e., on situations where some of the low-order Taylor coefficients in (16) vanish in dependence on k_0, u, and κ. In the neighborhood of such *degenerate points* in parameter space complex interactions of the two unstable modes can be expected. If we fix $\kappa\in(0,1)$ and $R\in\{0,1\}$, then we obtain local (1,2) interactions if the values of (k_0,u) are close to the line D_1 of Fig. 3. On D_1 we have the situation where the first and the second mode lose stability simultaneously at the same critical value of ν, i.e., $a_1=a_2=0$.

A. One-sided model ($R=0$)

The Taylor coefficients of $B^{(1)}$ and $B^{(2)}$ at $x=y=0$ and $\nu=\nu_c$ which govern the behavior of the (1,2) interactions are, following Ref. 17,

$$B^{(1)}_{x\nu}=\frac{\partial}{\partial\nu}a_1\,,\quad B^{(1)}_{xy}=a^{(1)}_{-1,2}\,,$$
$$B^{(2)}_{yyy}=\frac{6}{a^{(0)}_0a^{(4)}_4}(a^{(0)}_0a^{(4)}_4a^{(2)}_{-2,2,2}-a^{(4)}_4a^{(2)}_{0,2}a^{(0)}_{-2,2}$$
$$-a^{(0)}_0a^{(2)}_{-2,4}a^{(4)}_{2,2})\,, \tag{18}$$
$$B^{(2)}_{y\nu}=\frac{\partial}{\partial\nu}a_2\,,\quad B^{(2)}_{xx}=2a^{(2)}_{1,1}\,,$$

where the subscripts x, y, and ν denote partial derivatives. If one of these coefficients vanishes on D_1 we have a degeneracy giving rise to a certain type of (1,2) interaction.

The condition $a_1=a_2=\partial a_1/\partial\nu=0$ leads to a point P_1 in the (k_0,u) plane (see Fig. 3). This point exists for all values of κ and is a consequence of the geometrical structure of the neutral stability curve. On D_1, except for the point P_1, we have $B_{x\nu}^{(1)}>0$ for all $\kappa\in(0,1)$.

The condition $a_1=a_2=a_{-1,2}^{(1)}=0$ leads to a point $\tilde{Q}=(\tilde{k},\tilde{u})$ with

$$\tilde{k}^2=\frac{1-2\kappa}{2+5\kappa},\quad \tilde{u}=\frac{81}{4}\frac{(1+\kappa)(2-\kappa)(1-\kappa)\kappa^3}{(2+5\kappa)(1-2\kappa)^3}\ .$$

Because $\tilde{k}^2$ has to be positive, this point exists only for $\kappa<\frac{1}{2}$ and we see that $\tilde{k}\to 0$ and $\tilde{u}\to\infty$ for $\kappa\to\frac{1}{2}$. It is easily calculated that $\tilde{Q}$ coincides with P_1 for $\kappa=\frac{1}{2}(7-3\sqrt{5})\approx 0.1459$. On D_1 we have $B_{xy}^{(1)}<0$ above $\tilde{Q}$ and $B_{xy}^{(1)}>0$ below.

The expression for $B_{yyy}^{(2)}$ in terms of ν, κ, u, and k_0 is rather complicated, so it has not been possible to evaluate the conditions $a_1=a_2=B_{yyy}^{(2)}=0$ analytically. But numerical calculations showed that $B_{yyy}^{(2)}$ vanishes on D_1 at a point $\tilde{T}$ for $\kappa<\kappa_c\approx 0.0819$. On D_1 we have $B_{yyy}^{(2)}>0$ above and $B_{yyy}^{(2)}<0$ below the degenerate point $\tilde{T}$.

As to the remaining coefficients in (18), we got that on D_1 we have $B_{y\nu}^{(2)}>0$ and $B_{xx}^{(2)}<0$ for all $\kappa\in(0,1)$, especially they never vanish.

In the following we want to analyze the (1,2) interactions generated by the above degeneracies.

(i) At $(k_0,u)=\tilde{Q}$ we have $a_1=a_2=B_{xy}^{(1)}=0$. To get the normal form describing the bifurcation behavior of our system locally around the point $\tilde{Q}$ we still have to know, following Ref. 17, the sign of $B_{xyy}^{(1)}$, where

$$B_{xyy}^{(1)}=\frac{2}{a_0^{(0)}a_3^{(3)}}(a_0^{(0)}a_3^{(3)}a_{-2,1,2}^{(1)}-a_0^{(0)}a_{-2,3}^{(1)}a_{1,2}^{(3)} -a_3^{(3)}a_{-2,2}^{(0)}a_{0,1}^{(1)})\ ,$$

and the value of the model parameter

$$\rho=-\frac{B_{x\nu}^{(1)}|B_{yyy}^{(2)}|}{3|B_{xyy}^{(1)}B_{y\nu}^{(2)}|}\ . \tag{19}$$

Numerical evaluations show that $B_{xyy}^{(1)}<0$ and $-1<\rho<0$ for $(k_0,u)=\tilde{Q}$. This finally yields the unfolded codimension-two normal form

$$\begin{aligned}&-x(y^2-|\rho|\lambda+\alpha+\beta y)=0\ ,\\ &-x^2+y(y^2+\lambda)=0\ ,\end{aligned} \tag{20}$$

where α and β are the unfolding parameters and $\lambda\equiv\nu-\nu_c$. The solutions of (20) are curves in the (λ,x,y) space. For $x=0$ we obtain either the trivial solution $y=0$, corresponding to the planar interface, or a pure-mode branch S_y with $\lambda=-y^2$. For $x\neq 0$ we get the mixed-mode solution S_m with $\lambda=(y^2+\alpha+\beta y)/|\rho|$ and $x^2=y(y^2+\lambda)$. The projections into the (λ,y) plane of the six qualitatively different stable diagrams (for different values of α and β) are shown in Fig. 4. The $+,-$ signs denote degree of stability: $--$ means *stable*, and all others *unstable*. We see that the bifurcation of the second mode, the $x=0$, $\lambda=-y^2$ solution, is locally subcritical. But a numerical evaluation shows that $B_{yyyyy}^{(2)}$ is negative on D_1 for all values of κ, so that in all cases the pure-mode solution will finally bend forward, indicated in Fig. 4 by the dotted parts of the diagrams. In addition, we find in Figs. 4(a) and 4(b) at the point TB (standing for *tertiary bifurcation*) a tertiary Hopf bifurcation to time-periodic interface shapes. But our time-independent analysis does not allow any further statements on these time-dependent solutions and their stability. However,

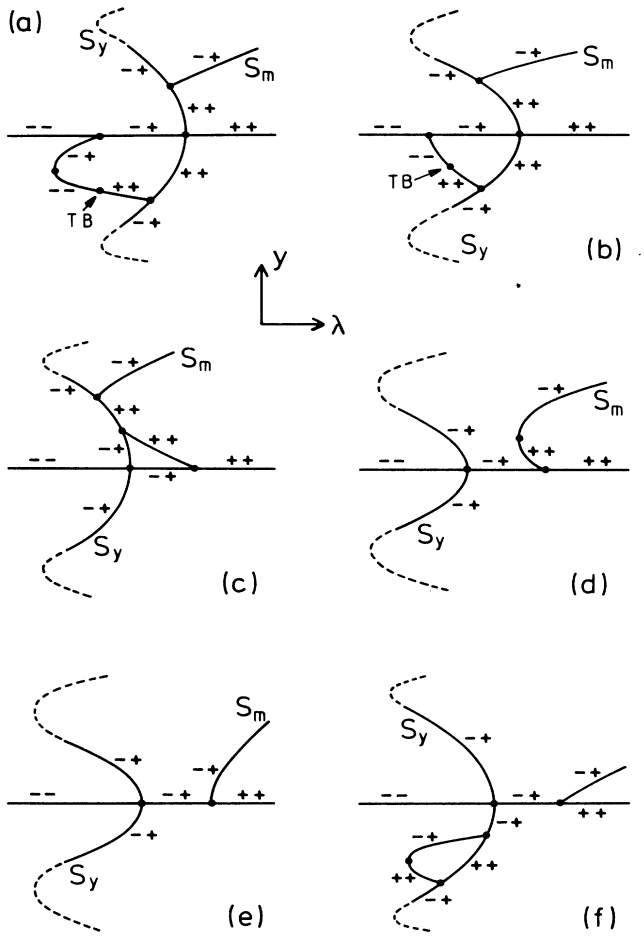

FIG. 4. Diagrams for the unfolded normal form (20) for (k_0,u) near $\tilde{Q}$, occurring for $R=0$. The solution curves are projected onto the (λ,y) plane. The $+,-$ signs indicate degree of stability, where $--$ means stable and all others unstable. (a)–(f) show the six qualitatively different diagrams for various values of the unfolding parameters α and β. In (a) and (b) we have at the point TB a tertiary bifurcation to time-periodic states. The dotted parts of the curves indicate that the branch S_y will finally bend forward because $B_{yyyyy}^{(2)}<0$ on D_1.

numerical analyses of Bennett, Brown, and Ungar[7] indicate that these time-periodic solutions bifurcate subcritically and are unstable.

Now it is possible to identify the different diagrams of Fig. 4 with values of (k_0,u) varying around $\tilde{Q}$. To this purpose we consider the curve $\tilde{K}_1$ defined by $a_1=B^{(1)}_{xxx}=0$, where

$$B^{(1)}_{xxx}=\frac{6}{a^{(0)}_0 a^{(2)}_2}(a^{(0)}_0 a^{(2)}_2 a^{(1)}_{-1,1,1}-a^{(2)}_2 a^{(1)}_{0,1} a^{(0)}_{-1,1} - a^{(0)}_0 a^{(1)}_{-1,2} a^{(2)}_{1,1}) .$$

The intersection point of $\tilde{K}_1$ with D_1 is, in our case, exactly the point $\tilde{Q}$. Furthermore, $\tilde{K}_1$ decides whether the bifurcation of the first mode is subcritical or supercritical. If now (k_0,u) lies in region a of Fig. 5, then the first mode bifurcates subcritically, because we are above $\tilde{K}_1$ and to the right of D_1, and the first mode bifurcates before the second mode, because we are to the right of D_1. Hence, the corresponding diagram has to be that of Fig. 4(a), because this is the only one with these two properties. Similarly we can establish the correspondences between regions b, c, d, e, and f in Fig. 5 and the diagrams (b), (c), (d), (e), and (f), in Fig. 4. Unfortunately, the dotted curve in Fig. 5 cannot be calculated explicitly, because it describes changes of the diagram off the trivial solution $x=y=0$.

(ii) For $(k_0,u)=\tilde{T}$, where $a_1=a_2=B^{(2)}_{yyy}=0$, we get the unfolded codimension-normal form

$$\begin{aligned} &-x(y-\lambda+\alpha)=0 , \\ &-x^2+y(-y^4+\lambda+\beta y^2)=0 , \end{aligned} \tag{21}$$

with the unfolding parameters α and β. The pure-mode solution S_y is given by $x=0$, $\lambda=y^2(y^2-\beta)$, the mixed-mode solution S_m by $\lambda=y+\alpha$, $x^2=y(-y^4+\lambda+\beta y^2)$. The projections into the (λ,y) plane of the six qualitatively different stable diagrams are shown in Fig. 6. With similar arguments as above we can establish again a correspondence between the different diagrams and the values of (k_0,u) varying around $\tilde{T}$. Let us consider the curve $\tilde{K}_2$, given by $a_2=B^{(2)}_{yyy}=0$, which intersects D_1 at $\tilde{T}$, see Fig. 7. $\tilde{K}_2$ decides whether the bifurcation of the pure-mode solution, corresponding to the mode number 2, is supercritical [for (k_0,u) below $\tilde{K}_2$] or subcritical (above $\tilde{K}_2$). So the regions a, b, c, d, e, and f of Fig. 7 correspond to the diagrams (a), (b), (c), (d), (e), and (f) of Fig. 6. Again, the dotted curve cannot be calculated explicitly.

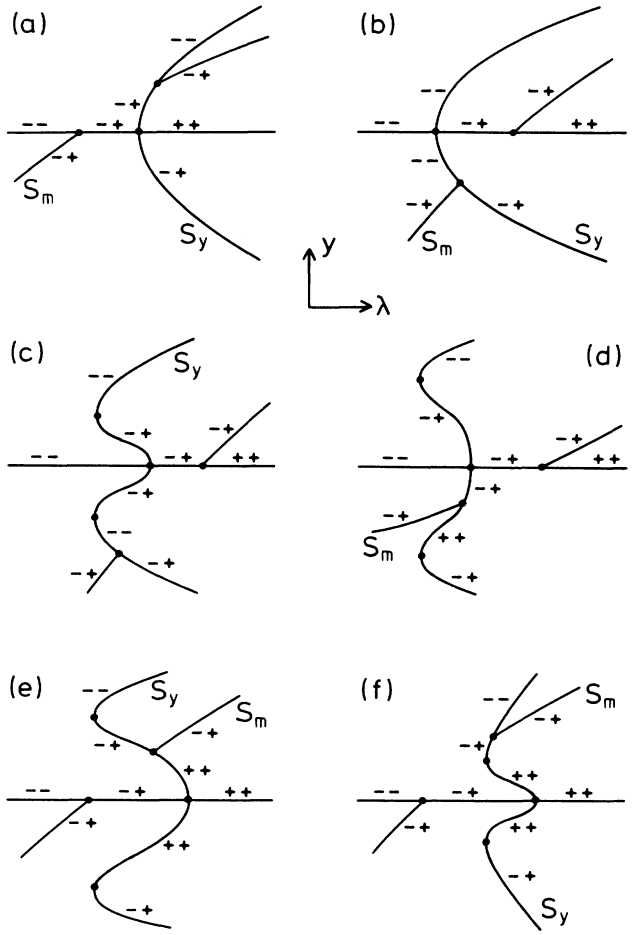

FIG. 6. Qualitatively different diagrams of the unfolded normal form (21) for (k_0,u) near $\tilde{T}$, occurring for $R=0$, and for (k_0,u) near $\tilde{T}_l$ or $\tilde{T}_r$, occurring for $R=1$. The curves are projected onto the (λ,y) plane.

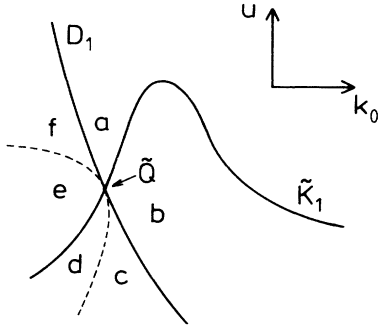

FIG. 5. Curves D_1 and $\tilde{K}_1$ near the point $\tilde{Q}$ in the (k_0,u) plane for $R=0$. On D_1 we have $a_1=a_2=0$, on $\tilde{K}_1$ we have $a_1=B^{(1)}_{xxx}=0$.

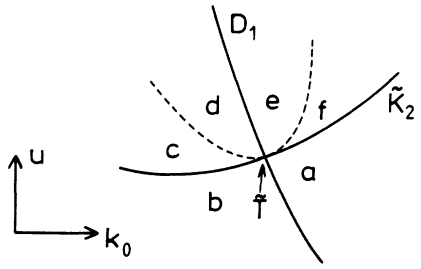

FIG. 7. Curves D_1 and $\tilde{K}_2$ near the point $\tilde{T}$ in the (k_0,u) plane for $R=0$. On $\tilde{K}_2$ we have $a_2=B^{(2)}_{yyy}=0$.

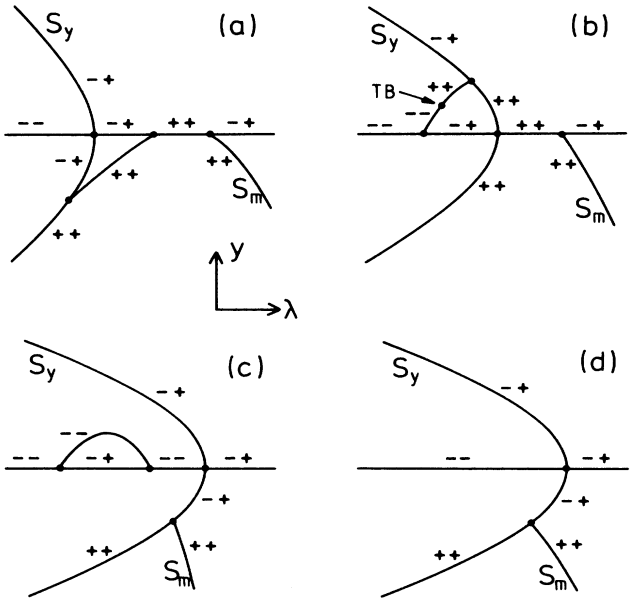

FIG. 8. Qualitatively different diagrams of the unfolded normal form (22) with $\varepsilon_2=+1$ and $\varepsilon_3=+1$ for (k_0,u) near P_1. In (b) we have at TB a tertiary bifurcation to time-periodic states.

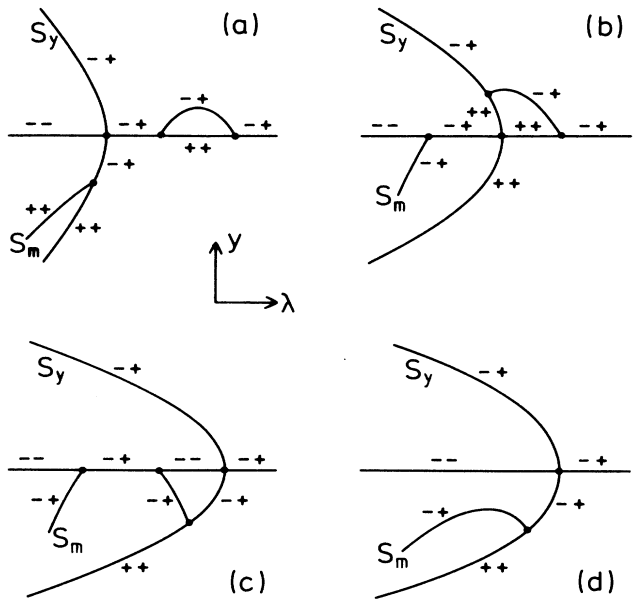

FIG. 9. Same as Fig. 8 for $\varepsilon_2=-1$ and $\varepsilon_3=+1$.

(iii) If $a_1=a_2=B_{xy}^{(1)}=0$, i.e., if $(k_0,u)=P_1$, then the corresponding normal form is given by

$$-x(y+\lambda^2+\alpha+\beta\lambda)=0\ ,$$
$$\varepsilon_2 x^2+y(\varepsilon_3 y^2+\lambda)=0\ , \tag{22}$$

with

$$\varepsilon_2=-\mathrm{sgn}(B_{xy}^{(1)}B_{xx}^{(2)}),\quad \varepsilon_3=\mathrm{sgn}(B_{yyy}^{(2)})\ .$$

If we take into account the above results about the zeros of $B_{xy}^{(1)}$ and $B_{yyy}^{(2)}$ on D_1 we get

$$\varepsilon_2=+1,\ \varepsilon_3=+1 \text{ for } 1.0>\kappa>0.1459\ ,$$
$$\varepsilon_2=-1,\ \varepsilon_3=+1 \text{ for } 0.1459>\kappa>0.0819\ ,$$
$$\varepsilon_2=-1,\ \varepsilon_3=-1 \text{ for } 0.0819>\kappa>0.0\ .$$

The pure-mode solution S_y is given by $x=0$, $\lambda=-\varepsilon_3 y^2$, the mixed-mode branch S_m by $y=-(\lambda^2+\alpha+\beta\lambda)$, $x^2=-\varepsilon_2 y(\varepsilon_3 y^2+\lambda)$. Because $B_{yyyyy}^{(2)}$ is negative, in all cases the pure-mode branch will finally bend forward and form a stable solution. The corresponding diagrams are depicted in Figs. 8–10, respectively. Again, we have the possibility of tertiary Hopf bifurcations. The correspondences of the different diagrams with values of (k_0,u) around P_1 are exactly those described in Ref. 10 for this degeneracy.

These are all codimension-two (1,2) interactions occurring in the frame of the system (7)–(13) with $R=0$. If we order the above results by values of κ we get the following scenario.

If κ is near the value 1.0, then the only degeneracy on D_1 is at the point P_1 and the bifurcations are described by (22) with $\varepsilon_2=+1$ and $\varepsilon_3=+1$ and Fig. 8. This is exactly the result obtained in Ref. 10, confirming that the approximation $J=$const in (4) corresponds in some sense to a limit of $\kappa\to 1$. Locally near D_1 the bifurcations are described by Fig. 13 of Ref. 10. If κ is decreased below the value $\frac{1}{2}$ the point $\tilde{Q}$ comes down from $(k_0,u)=(0,+\infty)$ and finally coalesces with P_1 at $\kappa=(7-3\sqrt{5})/2\approx 0.1459$. The bifurcations near $\tilde{Q}$ are

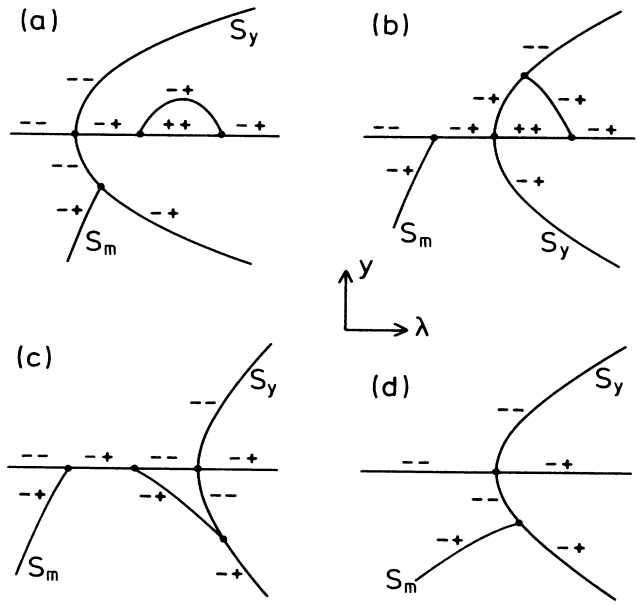

FIG. 10. Same as Fig. 8 for $\varepsilon_2=-1$ and $\varepsilon_3=-1$.

those of Fig. 4. For $0.1459>\kappa>0.0819$ again the only degeneracy is at P_1, the bifurcations now being those of Fig. 9. At $\kappa\approx 0.0819$ the point $\tilde{T}$ enters D_1 through P_1 and moves up along D_1 for κ decreasing further. But for $\kappa\to 0$ the k_0 coordinate of $\tilde{T}$ approaches $\sqrt{2}/4\approx 0.353\,55$, so the u coordinate remains finite. The bifurcations locally around $\tilde{T}$ are shown in Fig. 6. Additionally, the bifurcations at P_1 change for $\kappa<0.0819$, being described then by Fig. 10.

In the two special cases where $\tilde{Q}$ or $\tilde{T}$ coalesce with P_1 we should get codimension-three normal forms, describing a combination of the two underlying codimension-two degeneracies. The main effect of these degeneracies will be that in most cases the mixed-mode branch will reconnect the trivial solution for some $\nu>\nu_c$.

B. Symmetric model ($R=1$)

For the symmetric model we have to perform analog considerations as for the one-sided case. The Taylor coefficients governing the (1,2) interactions are still given by (18), but now with $R=1$ in the expressions for the $a^{(m)}_{r_1,\ldots,r_j}$ instead of $R=0$ (see Appendix). Considering the zeros of these Taylor coefficients, the situation is qualitatively nearly the same as for the one-sided model.

The condition $a_1=a_2=\partial a_1/\partial\nu=0$ again leads to a point P_1 in the (k_0,u) plane for all values of κ. Above P_1 we have again $B^{(1)}_{xy}>0$ on D_1.

As to $a_1=a_2=a^{(1)}_{-1,2}=0$, it can be satisfied for $\kappa<\tilde{\kappa}_c\approx 0.116\,19$ (this value is the solution of a polynomial of degree 10). Then we obtain two points $\tilde{Q}_l$ and $\tilde{Q}_r$ on D_1 which coalesce for $\kappa=\tilde{\kappa}_c$. For $\kappa>\tilde{\kappa}_c$ these points disappear, for decreasing κ the point $\tilde{Q}_r$, the one with the large k_0 value, coalesces with P_1 for $\kappa\approx 0.051\,523$, and for $\kappa\to 0$ we have $\tilde{Q}_l\to(0,+\infty)$. On D_1 we have $B^{(1)}_{xy}<0$ between $\tilde{Q}_l$ and $\tilde{Q}_r$ and $B^{(1)}_{xy}>0$ above $\tilde{Q}_l$ and below $\tilde{Q}_r$.

Numerical calculations show that $B^{(2)}_{yyy}$ vanishes on D_1 at two points $\tilde{T}_l$ and $\tilde{T}_r$ for $\kappa<\tilde{\tilde{\kappa}}_c\approx 0.028\,38$. For $\kappa\to 0$ we have $\tilde{T}_l\to(0,+\infty)$ and $\tilde{T}_r\to(\sqrt{2}/4,0)$, especially $\tilde{T}_r$ never coalesces with P_1. On D_1 we have $B^2_{yyy}>0$ between $\tilde{T}_l$ and $\tilde{T}_r$ and $B^{(2)}_{yyy}<0$ above $\tilde{T}_l$ and below $\tilde{T}_r$.

The remaining coefficients $B^{(2)}_{yy}$ and $B^{(2)}_{xx}$ never vanish on D_1, we have $B^{(2)}_{yy}>0$ and $B^{(2)}_{xx}<0$ for all $\kappa\in(0,1)$.

This now leads to the following (1,2) interactions in the symmetric model.

(i) At the points $\tilde{Q}_{l,r}$, where $a_1=a_2=B^{(1)}_{xy}=0$, we have $B^{(1)}_{xyy}<0$ and $-1<\rho<0$, where ρ is the model parameter given by (19). Together with the above results this yields the unfolded codimension-two-normal form

$$\begin{aligned} &-x(y^2-|\rho|\lambda+\alpha+\beta y)=0\,,\\ &-x^2+y(-y^2+\lambda)=0\,, \end{aligned} \tag{23}$$

where α and β are again the unfolding parameters. The resulting diagrams are shown in Fig. 11. The main difference to the corresponding diagrams in the one-sided model is that the pure-mode solution now bifurcates supercritically and that the tertiary Hopf bifurcation occurs in a different situation. In the same way as in the one-sided model we can establish correspondences between the different diagrams and regions around the points $\tilde{Q}_{l,r}$ in the (k_0,u) plane, the result is shown in Fig. 12.

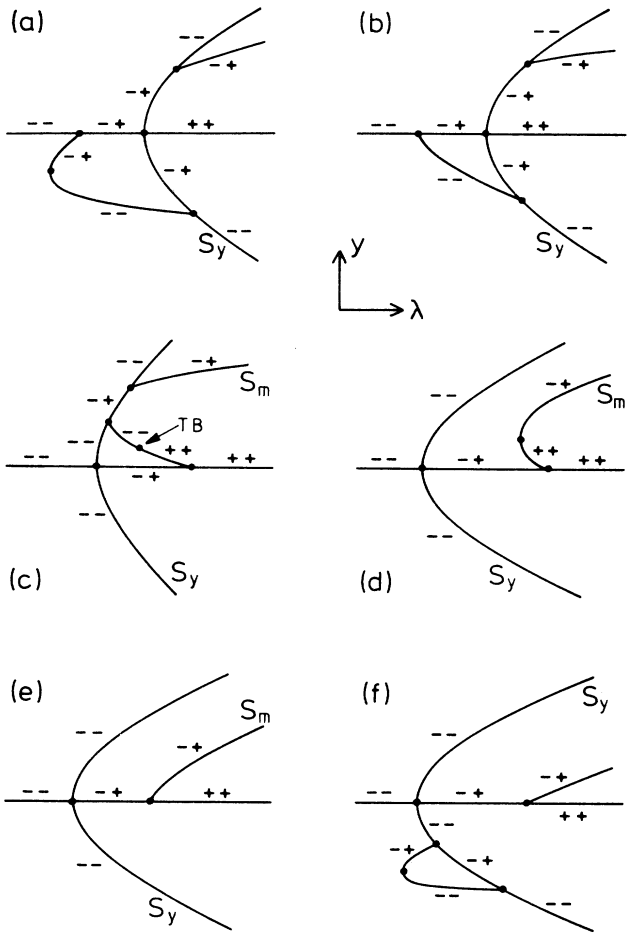

FIG. 11. Diagrams for the unfolded normal form (23) for (k_0,u) near $\tilde{Q}_l$ or $\tilde{Q}_r$, occurring for $R=1$. The solution curves are projected onto the (λ,y) plane. In (c) we have at TB a tertiary bifurcation to time-periodic states.

(ii) For $(k_0,u)=\tilde{T}_{l,r}$, where $a_1=a_2=B^{(2)}_{yyy}=0$, we get the unfolded codimension-two normal form

$$\begin{aligned} &-x(y-\lambda+\alpha)=0\,,\\ &-x^2+y(-y^4+\lambda+\beta y^2)=0\,, \end{aligned} \tag{24}$$

which is identical with (21), so that the different diagrams are those of Fig. 6. The correspondences to the neighborhoods of $\tilde{T}_{l,r}$ are shown in Fig. 13.

(iii) For $a_1=a_2=B^{(1)}_{xy}=0$, i.e., for $(k_0,u)=P_1$, the unfolded normal form is given by

$$\begin{aligned} &-x(y+\lambda^2+\alpha+\beta\lambda)=0\,,\\ &\varepsilon_2 x^2+y(\varepsilon_3 y^2+\lambda)=0\,, \end{aligned} \tag{25}$$

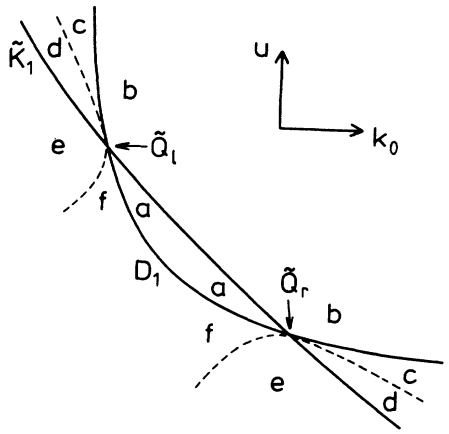

FIG. 12. Curves D_1 and $\tilde{K}_1$ near the points $\tilde{Q}_l$ and $\tilde{Q}_r$ in the (k_0,u) plane for $R=1$.

with

$$\varepsilon_2=-\mathrm{sgn}(B_{xy}^{(1)}B_{xx}^{(2)}),\quad \varepsilon_3=\mathrm{sgn}(B_{yyy}^{(2)})\ ,$$

being identical with (22). With the above results about the signs of $B_{xy}^{(1)}$ and $B_{yyy}^{(2)}$ on D_1 we get

$$\varepsilon_2=+1,\quad \varepsilon_3=-1\quad \text{for } 1.0>\kappa>0.051\,523\ ,$$

$$\varepsilon_2=-1,\quad \varepsilon_3=-1\quad \text{for } 0.051\,523>\kappa>0.0\ .$$

The diagrams for the first case are shown in Fig. 14, those for the second case are the same as in Fig. 10.

These are all local codimension-two (1,2) interactions occurring in the system (7)–(13) with $R=1$. For decreasing values of κ we have the following picture.

If κ is near 1.0 the only degeneracy on D_1 is at P_1, the corresponding diagrams are those of Fig. 14. If κ is decreased below $\tilde{\kappa}_c\approx 0.116\,19$, then the two points $\tilde{Q}_l$ and

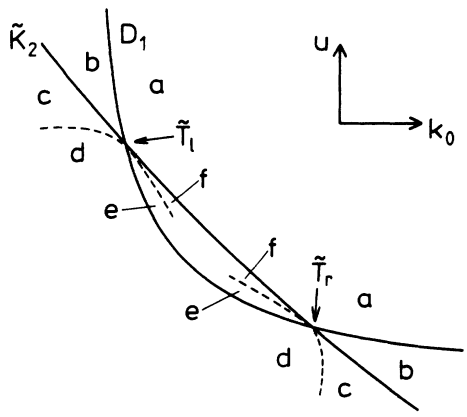

FIG. 13. Curves D_1 and $\tilde{K}_2$ near the points $\tilde{T}_l$ and $\tilde{T}_r$ in the (k_0,u) plane for $R=1$.

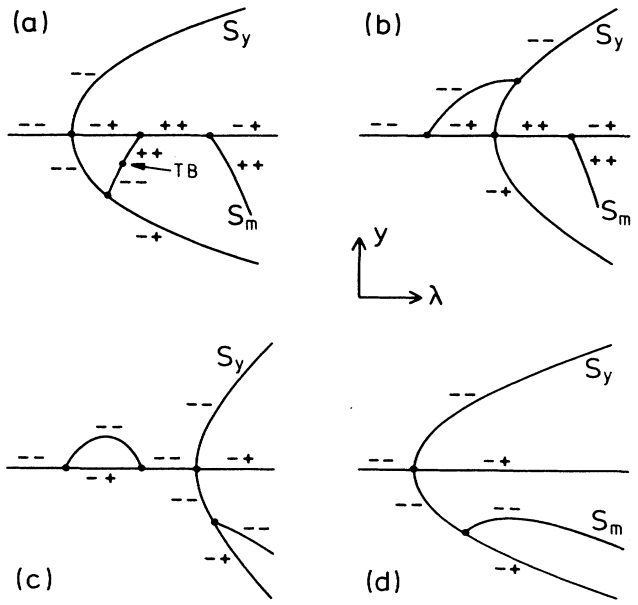

FIG. 14. Diagrams for the unfolded normal form (25) with $\varepsilon_2=+1$ and $\varepsilon_3=-1$ for (k_0,u) near P_1.

$\tilde{Q}_r$ appear on D_1, for $\kappa=\tilde{\kappa}_c$ they coalesce. For κ decreasing further, $\tilde{Q}_l$ moves up on D_1 and $\tilde{Q}_r$ moves down. $\tilde{Q}_l$ approaches $(k_0,u)=(0,+\infty)$ for $\kappa\to 0$ and $\tilde{Q}_r$ reaches P_1 at $\kappa\approx 0.051\,523$. In the latter case we should get a codimension-three normal form, describing a combination of the two underlying degeneracies. The diagrams near $\tilde{Q}_l$ and $\tilde{Q}_r$ are given in Fig. 11. If κ is decreased below $\tilde{\tilde{\kappa}}_c\approx 0.028\,38$, then the points $\tilde{T}_l$ and $\tilde{T}_r$ appear on D_1. For $\kappa\to 0$ the point $\tilde{T}_l$ moves up to infinity and $\tilde{T}_r$ approaches some point on D_1. The diagrams are shown in Fig. 6.

VI. DISCUSSION

In the frame of system (7)–(13) we have analyzed all local codimension-two (1,2) interactions for $R=0$ and $R=1$, describing the bifurcation of a planar interface to stationary cellular morphologies. We found many more different types of bifurcation than in the simpler model of Ref. 10, which is valid only for values of κ near 1.0. The main features of our diagrams are various types of hysteresis as, e.g., in Figs. 4(a), 6(c), and 11(f), and tertiary Hopf bifurcations as in Figs. 4(b), 11(c), and 14(a). The way in which the system bifurcates depends on the values of the system parameters k_0, u, and κ.

In numerical simulations one can see in the bifurcation diagrams *folds* in the mixed-mode solution.[8,9] This is a situation where the mixed-mode branch bifurcates supercritically off the trivial solution, then bends back via a limit point and finally connects with the pure-mode branch in a secondary bifurcation point. This sort of diagram occurs in the degeneracy defined by $a_1=a_2=a_{1,1}^{(2)}=0$ which, as we have seen, does not exist in the system (7)–(13). So this diagram is not a local one,

i.e., for (k_0,u) near enough to the curve D_1 it does not occur. But, if (k_0,u) has a certain distance to the curve D_1, such that it is outside the range of validity of the local analysis used in this paper, then such a diagram with a fold indeed can be possible. I tried to verify this by using a Taylor expansion of (16) up to order 2 in ν and 5 in x and y, such that each equation in (16) had 27 terms. The coefficients and the diagrams then had been computed numerically. For values of (k_0,u) near D_1 I obtained exactly the local diagrams described above, but when the distance of (k_0,u) to D_1 was increased, the Taylor expansion broke down before the fold showed up. In this sense, the occurrence of these folds is a nonlocal event.

In a recent paper, Kessler and Levine[9] showed that the limit $R\to 0$ is not a proper one. The easiest way to see that is the following: If the interface is not planar, then the solute concentration along the interface is not constant by virtue of (9) and (13). Therefore the solute concentration in the solid just below the interface is inhomogeneous in the ξ direction. For $R\neq 0$ these inhomogeneities are equalized by diffusion on the way to $\eta=-\infty$, thus that the condition (12) is fulfilled. If $R=0$, then (8) simply becomes a traveling wave equation, the lateral inhomogeneity in the solid is frozen and (12) cannot be met. On the other hand, in my calculations R never acted as some sort of singular perturbation of the case $R=0$. The reason for this is that $p(n)$ given in (17) and its ν derivatives have proper limits for $R\to 0$. Thus all the coefficients $a^{(n)}_{r_1,\ldots,r_m}$ and eventually all the Taylor coefficients of (16) possess proper limits for $R\to 0$. The reason for this inconsistency is that the mismatch between the cases $R=0$ and $R>0$ occurs for $\eta\to-\infty$, i.e., far away from the interface, so that the latter is not affected by this problem. So the limit $R\to 0$ is not a proper one for the solute concentration field on the whole sample, but it is a proper limit if only the interface is considered.

It would be very desirable to extend the above analysis to the case of general $R\in[0,1]$. Then it should be possible to find points in the (k_0,u,κ,R) parameter space where some of the degeneracies found in the cases $R=0$ and 1 come together, giving rise to (1,2) interactions of codimension higher than two. Perhaps it would be possible to find an *organizing center*, i.e., a point where all the above degeneracies meet, satisfying the condition $a_1=a_2=\partial a_1/\partial\nu=a^{(1)}_{-1,2}=B^{(2)}_{yyy}=0$. But at the moment such an analysis is out of the scope of the computer system I have access to, because for $R\neq 0,1$ the complexity of the equations involved increases dramatically. This is due to the fact that we have in (17) $p(n)=0$ for $R=0$ and $p(n)=q(n)-\nu$ for $R=1$, thus $p(n)$ can be eliminated in these cases. Presently, the only way to find such higher degeneracies seems to be a numerical search in the (k_0,u,κ,R) space.

Finally, it should be emphasized again that the (1,2) interactions are only part of the truth. For an arbitrary experimental setup it will usually not be the mode number 1 which becomes unstable first. Especially if the width of the sample is much larger than the wavelength of the evolving interface structures, then the (1,2) interactions are not appropriate to describe the corresponding bifurcation behavior. Therefore it is necessary to extend the above analysis to general $(n,n+1)$ interactions as in the simpler model with $J=\text{const}$ in Ref. 10.

ACKNOWLEDGMENTS

It is a pleasure to acknowledge stimulating discussions with D. Armbruster, G. Dangelmayr, and W. Güttinger, and the support of the Stiftung Volkswagenwerk.

APPENDIX

In this appendix we give explicit formulas for the coefficients $a^{(n)}_{r_1,\ldots,r_m}$ in Eq. (14). We have

$$
\begin{aligned}
a^{(n)}_{r_1,r_2,\ldots,r_m} = {} & \frac{1}{\mu(r_1,\ldots,r_m)}\{F_m(r_1,\ldots,r_m)[q(n)-\nu(1-\kappa)]+RG_m(r_1,\ldots,r_m)p(n)\} \\
& -\sum_{\eta=0}^{m-1}\sum_{a\in P_\eta(N_m)}\sum_{(n_1,n_2,\ldots,n_{m-\eta})\in\mathcal{M}_{N_m}\setminus a}\frac{1}{\mu(r_{a_1},\ldots,r_{a_\eta})} \\
& \times\Bigg[(-1)^{m-\eta-1}F_\eta(r_{a_1},\ldots,r_{a_\eta})q^{m-\eta-1}(r_{a_1}+\cdots+r_{a_\eta}) \\
& \times\Bigg[\frac{1}{(m-\eta)!}[q(r_{a_1}+\cdots+r_{a_\eta})-\nu(1-\kappa)]q(r_{a_1}+\cdots+r_{a_\eta}) \\
& +\frac{1}{(m-\eta-1)!}n_1(r_{a_1}+\cdots+r_{a_\eta})uz\Bigg] \\
& -RG_\eta(r_{a_1}+\cdots+r_{a_\eta})p^{m-\eta-1}(r_{a_1}+\cdots+r_{a_\eta}) \\
& \times\left[\frac{1}{(m-\eta)!}p^2(r_{a_1}+\cdots+r_{a_\eta})+\frac{1}{(m-\eta-1)!}n_1(r_{a_1}+\cdots+r_{a_\eta})uz\right]\Bigg],
\end{aligned}
$$

where

$$\sum_{i=1}^{m} r_i = n, \quad P_\eta(N_m) = \{M \subset N_m \mid |M| = \eta\}, \quad N_m = \{1,2,3,\ldots,m\} .$$

For $b \in P_\eta(N_m)$ we set $\tilde{b} \equiv (\tilde{b}_1, \ldots, \tilde{b}_\eta)$ with $\tilde{b}_i \in b$ and $\tilde{b}_1 < \tilde{b}_2 < \cdots < \tilde{b}_\eta$.

$$\mathcal{M}_b \equiv \{r_{(\pi\tilde{b})_1}, \ldots, r_{(\pi\tilde{b})_\eta}) \mid \pi \in S_\eta\} ,$$

where S_η is the group of permutations of η elements. Furthermore, we have

$$\mu(r_1, r_2, \ldots, r_\eta) = \prod_{r \in \mathcal{R}(r_{a_1}, \ldots, r_{a_\eta})} |J(r; r_1, \ldots, r_\eta)|! ,$$

$$\mathcal{R}(r_1, \ldots, r_\eta) = \{r_1, \ldots, r_\eta\}, \quad |\mathcal{R}| < \eta \quad \text{if } r_i = r_j \quad \text{for } i \neq j$$

$$J(r; r_1, \ldots, r_\eta) = \{i \in N_\eta \mid r = r_i\} ,$$

$$q(m) = \frac{\nu}{2} + \left[\frac{\nu^2}{4} + u m^2 k_0^2\right]^{1/2}, \quad p(m) = -\frac{\nu}{2R} + \left[\frac{\nu^2}{4R^2} + u m^2 k_0^2\right]^{1/2} .$$

For the functions F_m and G_m the following recursions are valid:

$$F_0 = \frac{1-\kappa}{\kappa}, \quad F_1(m) = \nu\frac{1-\kappa}{\kappa} - 1 - m^2 k_0^2 ,$$

$$F_m(r_1, r_2, \ldots, r_m) = -(-\nu)^m \frac{1-\kappa}{\kappa} - \sum_{\eta=1}^{m-1} \sum_{a \in P_\eta(N_m)} F_\eta(r_{a_1}, \ldots, r_{a_\eta})[-q(r_{a_1} + \cdots + r_{a_\eta})]^{m-\eta}$$

$$- \tfrac{1}{2}[1 + (-1)^{m+1}] u^{(m-1)/2} k_0^{m+1} (r_1 + r_2 + \cdots + r_m) r_1 r_2 \cdots r_m \frac{m!!(m-1)!}{\left[\frac{m-1}{2}\right]! 2^{(m-1)/2}} ,$$

$$G_0 = 0, \quad G_1(m) = -\kappa(1 + m^2 k_0^2) ,$$

$$G_m(r_1, r_2, \ldots, r_m) = -\sum_{\eta=1}^{m-1} \sum_{a \in P_\eta(N_m)} G_\eta(r_{a_1}, \ldots, r_{a_\eta}) p^{m-\eta}(r_{a_1} + \cdots + r_{a_\eta})$$

$$- \tfrac{1}{2}[1 + (-1)^{m+1}] \kappa u^{(m-1)/2} k_0^{m+1} (r_1 + r_2 + \cdots + r_m) r_1 r_2 \cdots r_m \frac{m!!(m-1)!}{\left[\frac{m-1}{2}\right]! 2^{(m-1)/2}} .$$

Especially we have

$$a_n^{(n)} = F_1(n) q(n) - F_1(n)\nu(1-\kappa) + R G_1(n) p(n) - \nu^2(1-\kappa) ,$$

$$a_{0,n}^{(n)} = \nu(\nu - q(n)) ,$$

$$a_{-n,n}^{(0)} = 2R G_1(n)[p^2(n) - u n^2 k_0^2] ,$$

$$a_{-n,2n}^{(n)} = \nu^3\frac{1-\kappa}{\kappa} - \nu^2\frac{1-\kappa}{\kappa} q(n) - F_1(2n) q^2(2n) + F_1(2n) q(n) q(2n) + 2u n^2 k_0^2 F_1(n) + 2u n^2 k_0^2 F_1(2n)$$
$$+ R G_1(2n) p^2(2n) - R G_1(2n) p(n) p(2n) - 2R u n^2 k_0^2 [G_1(n) + G_1(2n)] ,$$

$$a_{n,n}^{(2n)} = \nu^3\frac{1-\kappa}{\kappa} - \nu^2\frac{1-\kappa}{\kappa} q(2n) - F_1(n) q^2(n) + F_1(n) q(n) q(2n) - u n^2 k_0^2 F_1(n) + R G_1(n) p^2(n)$$
$$- R G_1(n) p(n) p(2n) + R u n^2 k_0^2 G_1(n) ,$$

$$a_{-n,n,n}^{(n)} = \nu^4\frac{1-\kappa}{2\kappa} - \nu^3\frac{1-\kappa}{2\kappa} q(n) + \nu^2\frac{1-\kappa}{2\kappa} q^2(2n) - \nu^2\frac{1-\kappa}{2\kappa} q(n) q(2n) - \nu^2\frac{1-\kappa}{2\kappa} u n^2 k_0^2 - 2\nu^2 F_1(n) q(n)$$
$$+ 2\nu F_1(n) q^2(n) - F_1(n) q(n) q^2(2n) + F_1(n) q^2(n) q(2n) + u n^2 k_0^2 F_1(n) q(n) + \tfrac{3}{2} u n^4 k_0^4 q(n)$$
$$- \tfrac{3}{2}\nu(1-\kappa) u n^4 k_0^4 + R G_1(n) p^2(n) p(2n) - R G_1(n) p(n) p^2(2n) + R u n^2 k_0^2 G_1(n) p(n)$$
$$+ \tfrac{3}{2}\kappa R u n^4 k_0^4 p(n) .$$

[1]J. S. Langer, Rev. Mod. Phys. **52**, 1 (1980).
[2]S. de Cheveigné, C. Guthman, and M. M. Lebrun, J. Phys. (Paris) **47**, 2095 (1986).
[3]J. Bechhoefer and A. Libchaber, Phys. Rev. B **35**, 1393 (1987).
[4]B. Caroli, C. Caroli, and B. Roulet, J. Phys. (Paris) **43**, 1767 (1982).
[5]M. Kerszberg, Phys. Rev. B **27**, 6796 (1983).
[6]L. H. Ungar and R. A. Brown, Phys. Rev. B **29**, 1367 (1984).
[7]M. J. Bennett, R. A. Brown, and L. H. Ungar, in *The Physics of Structure Formation,* edited by W. Güttinger and G. Dangelmayr (Springer, Berlin, 1987).
[8]N. Ramprasad, M. J. Bennett, and R. A. Brown, Phys. Rev. B **38**, 583 (1988).
[9]D. A. Kessler and H. Levine, Phys. Rev. A **39**, 3041 (1989).
[10]P. Haug, Phys. Rev. A **35**, 4364 (1987).
[11]P. Haug, Ph.D. thesis, University of Tübingen, Tübingen, Germany, 1988.
[12]M. Neveling, D. Lang, P. Haug, W. Güttinger, and G. Dangelmayr, in *The Physics of Structure Formation,* edited by W. Güttinger and G. Dangelmayr (Springer, Berlin, 1987).
[13]P. Haug, in *Synergetics, Order and Chaos,* edited by M. G. Velarde (World Scientific, Singapore, 1988).
[14]*The Physics of Structure Formation,* edited by W. Guttinger and G. Dangelmayr (Springer, Berlin, 1987).
[15]M. Golubitsky and D. Schaeffer, *Singularities and Groups in Bifurcation Theory* (Springer, New York, 1985), Vol. I; M. Golubitsky, I. Stewart, and D. G. Schaeffer, *Singularities and Groups in Bifurcation Theory* (Springer, New York, 1988), Vol. II.
[16]D. Schaeffer and M. Golubitsky, Commun. Math. Phys. **69**, 209 (1979).
[17]D. Armbruster and G. Dangelmayr, Math. Proc. Cambridge Philos. Soc. **101**, 167 (1987).